

THE POST PEAK RESPONSE OF CONCRETE FOR DYNAMIC TENSILE LOADING

I.Vegt^a

^aFaculty of Civil Engineering and Geosciences, Delft University of Technology, The Netherlands
I.Vegt@tudelft.nl

J. Weerheijm^{a,b,*}

^a Faculty of Civil Engineering and Geosciences, Delft University of Technology, The Netherlands ^bTNO
Defence, Security and Safety, The Netherlands jaap.weerheijm@tno.nl (Corresponding Author)

ABSTRACT

The mechanical response of concrete is represented in the load-deformation curve which shows the response up to maximum strength as well as the post-peak response up to complete failure. Dynamic tests exhibit an extensive rate effect on the tensile strength beyond loading rates of about 50 GPa/s (strain rates > 1/s). Whether the apparent strength increase is real material response or that it is affected by inertia effects at macro and micro scale is under discussion. The authors contributed to discussion by their instrumented SHB and spalling tests. By measuring the deformation in the failure zone directly and real time, the contribution of inertia could be demonstrated and estimated quantitatively. The direct measurement of the deformation also holds for the post-peak process. Data on the post-peak response and the analysis of the data will be presented in this paper.

In the experimental programme a reference concrete was tested at three moisture levels, i.e dry, normal and saturated. Static, SHB and spalling tests were performed so data on a wide range of loading rates was obtained. The analysis presented in the paper addresses the effects of (i) the pore saturation level, (ii) the amount of micro cracks in the failure zone, (iii) the limited crack velocity, (iv) the micro inertia effect on crack initiation and (v) the structural inertia of failure zone. The latter proved to be only relevant during the pre- and post peak micro cracking process at the high loading rate regime.

KEYWORDS

Concrete, rate effects, fracture energy, experiments, structural inertia, micro-inertia, constitutive law.

INTRODUCTION

Experiments show that concrete response is rate dependent in tension. Especially for loading rates beyond 50GPa/s increased rate effects are observed for strength as well as fracture energy. Nowadays there is consensus in literature on the mechanisms of the observed rate dependency in tension strength. First of all there is the overall structural response of the concrete specimen, so its geometry, size and the structural inertia of the specimen have to be taken into account analysing the test result. These effects are not related to the material response itself and will not be discussed in this paper.

The material dynamic response mechanisms are related to (i) the pore structure and moisture contents, (ii) inertia effects around the (micro) cracks affecting crack initiation and propagation (i.e denoted as micro inertia effects) and (iii) (structural) inertia effect of the softening zone, see e.g.(Reinhardt,1990; Cotsovos, 2007; Ožbolt 2012 and Weerheijm et al. 2013). The question is how to quantify these individual contributions and how they depend on the strain rate. Directly related is the discussion in literature how to interpret the test data to derive the rate dependency that should be implemented in the constitutive equation for concrete.



This work is licensed under the Creative Commons Attribution 4.0 International License.
To view a copy of the license, visit <https://creativecommons.org/licenses/by/4.0/>.

The authors performed extensive test series at static, intermediate and high loading rates for normally cured concrete as well as dried and saturated concrete. The aim was to study the rate effect on strength as well as the softening behaviour and the fracture energy. Therefore the diagnostics were dedicated to directly measure the strength, but also the deformation of the fracture zone, in order to reconstruct the full stress-deformation relation at the different loading rates. In addition the width of the fracture zone and the crack distribution were determined using microscopy. The first part of the paper summarizes the testing devices, the diagnostics and the test data. More details are given in (Weerheijm et al., 2009, 2011, 2013 and Vegt 2015 thesis). In the second part the focus is on the structural inertia of the softening zone. The effect on the observed strength is determined by analysing the pre-peak response and the effect on the fracture energy follows from the post-peak response analysis.

EXPERIMENTAL PROGRAMME

Testing devices and material composition

Experiments are conducted at three different loading rates; static loading rate (10^{-4} GPa/s) as a reference, medium loading rate with a Split Hopkinson Bar (SHB) set-up (≈ 50 GPa/s) and high loading rates with a Modified Split Hopkinson Bar (MSHB) (> 1000 GPa/s), see Figure 1.

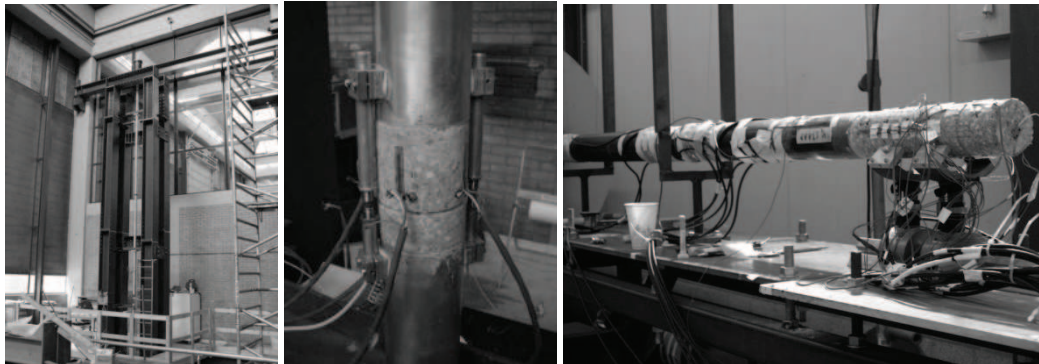


Figure 24 (left) The Split Hopkinson Bar (SHB) at the Delft University of Technology; (middle) detail of the glued specimen and measurement system of the SHB and (right) the Modified Split Hopkinson Bar set-up at TNO Defence, Security and Safety.

The cylindrical concrete specimens have a diameter of 74mm. The length of the specimens for the static and Split Hopkinson Bar (SHB) tests is 100mm. The specimens for the high loading rate tests have a length of 300mm. For the concrete mixture a Portland cement (CEM I 32.5R) is used. The maximum aggregate size is 8mm. The three curing conditions were:

- “Normal” condition: specimens are stored under controlled conditions of 20°C and 50% relative humidity (RH);
- “Wet” condition: specimens are submersed in water;
- “Dry-50” condition: specimens are dried in an oven of 50°C and 15% RH;

For the normal curing condition the average compressive cube strength and tensile splitting strength at 28 days is 48MPa and 3.4MPa. The compressive-, tensile splitting strength and Young’s modulus at 42 days are 52MPa, 3.6MPa and 35.1GPa respectively.

Diagnostics SHB and MSHB tests

In the SHB set-up the tensile stress wave is generated using a drop weight, which slides along the lower bar and hits an anvil at the end. In the SHB set-up the strains are measured at the upper bar, while the total and elastic deformations are measured directly on the notched specimens with LVDT’s (Linear Variable Differential Transducers) and strain gauges respectively. The signals are synchronised and combined to reconstruct the desired stress-deformation curve. The strength and fracture energy are quantified by this curve.

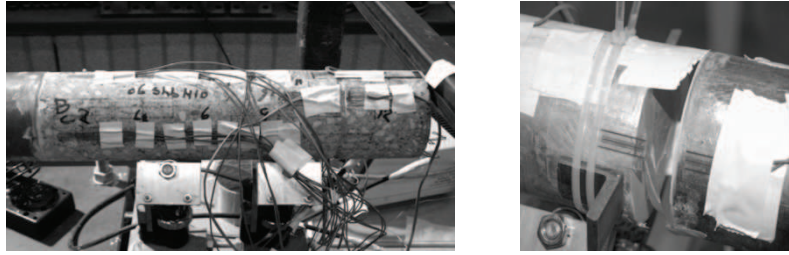


Figure 25 (left) The concrete specimen of the MSHB with strain gauges.

Figure 26 (right) Detail of the deformation measuring device with strain gauges on a supporting foil; (Photo shows the broken gauge after full separation).

For the high loading rate regime (>1000 GPa/s) the Modified Split Hopkinson Bar (MSHB) set-up is used. The MSHB is based on the principle of spalling.

The measurement set-up of the MSHB is comparable to the set-up of the SHB. The transmitted pressure wave in the concrete specimen, the wave propagation and the reflection process are recorded with strain gauges distributed along the notched specimen (Figure 2). The loading rate and applied load are derived from the strain measurements on the steel bar and the specimen. The resulting stress at the failure zone (notch) is determined using the uniaxial wave theory to quantify the wave interaction process [Vegt et al. 2006, 2007 and 2015]. To derive the desired stress-deformation curve, it is necessary to determine the deformation of the fracture zone directly. New deformation measuring devices have been developed (Figure 3), which are almost weightless and can measure deformations at very high loading rates. The measured deformations at the notch are combined with the resulting stresses in the notch to obtain the desired stress-deformation curve at high loading rates.

The width of the fracture zone and crack data.

To obtain quantitative results on crack lengths and widths of the fracture zone, the crack patterns are digitalized. The cracks are subdivided into (see Figure 4 left) : 1) the macro crack, which is the crack where physical separation of the two parts of the specimen has taken place, 2) the connected micro cracks, which are connected to the macro crack and 3) the isolated micro cracks, which are not connected to the macro crack but found isolated in the concrete sample and determine the width of the fracture zone. Figure 4(left) shows a crack pattern and illustrates the crack categories and the width of the fracture zones for the macro crack (WFZ_{macro} , blue), macro and connected micro cracks ($WFZ_{ConMicro}$, green) and the total width of the fracture zone ($WFZ_{micro} = L_{FZ}$, red). The crack lengths are measured and given in Figure 4(right) and Table 1.

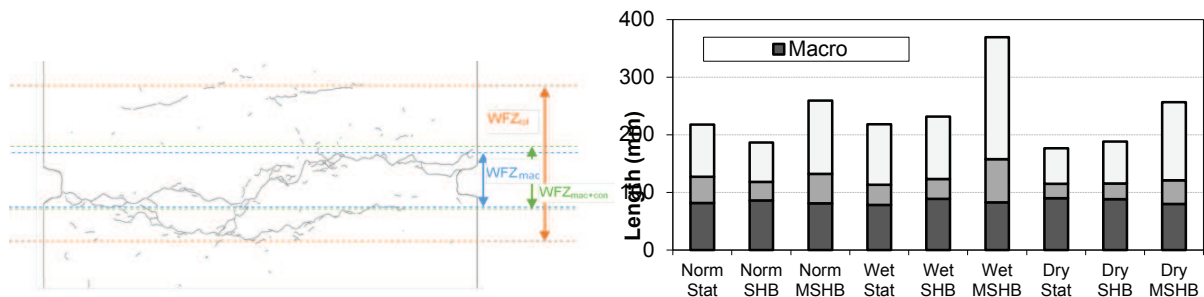


Figure 27 (left) Example of crack pattern and definition crack categories and (right) crack data summary

The data shows that the length of the macro crack varies only slightly, but the amount of micro cracking increases significantly for the high loading rate and also the total width of the fracture zone increases. At the high loading rate concrete behaves less brittle. For the “wet curing condition” this behaviour is most pronounced.

Table 3 Data on fracture patterns

$\dot{\sigma}$ GPa/s	Dry				normal				wet			
	l_{FZ} mm	l_{mac} mm	$l_{mic,tot}$ mm	DIF l_{micro}	l_{FZ} mm	l_{mac} mm	$l_{mic,tot}$ mm	DIF l_{micro}	l_{FZ} mm	l_{mac} mm	$l_{mic,tot}$ mm	DIF l_{micro}
10^{-4}	8.7	90	86	1.0	6.7	82	136	1.0	6.0	78	140	1.0
40	8.8	88	100	1.2	8.1	86	100	0.7	9.6	88	143	1.0
1700	43.7	80	177	2.1	19.1	81	178	1.3	47.5	83	288	2.1

l_{FZ} = width fracture process zone; l_{mac} = length macro cracks; $l_{mic,tot}$ =total length of all micro cracks in fracture process zone; DIF= ratio total length micro cracks for dynamic and static case

In (Vegt, 2015) the experiments and the data is presented and analysed in detail for all curing conditions and loading rates. In the next pages of this paper structural inertia effects of the fracture zone are discussed for the concrete material cured under normal conditions.

THE APPARENT STRENGTH

The effect of structural inertia of the fracture zone on the dynamic strength is determined by the deformation rate in the pre-peak phase of the stress-deformation curve. The question is when structural inertia effects obscure the true material response? Various researchers addressed this issue a.o. Cotsovos [3] and Ozbolt [10,11,25]. Because in our tests the stress conditions, the deformation and the width of the fracture zone are known, a reconstruction of the failure process can be made. We first discuss the results for the MSHB tests. The deformation of the fracture zone is recorded by the newly developed deformation gauges. With the deformation of the fracture zone and the measured strains at several locations of the specimen, the stress-deformation curve was reconstructed. An example of the stress, $\sigma(t)$, the deformation of the fracture zone $\delta(t)$, and the corresponding deformation velocity $\dot{\delta}(t)$ for a MSHB tests is presented in Figure 5.

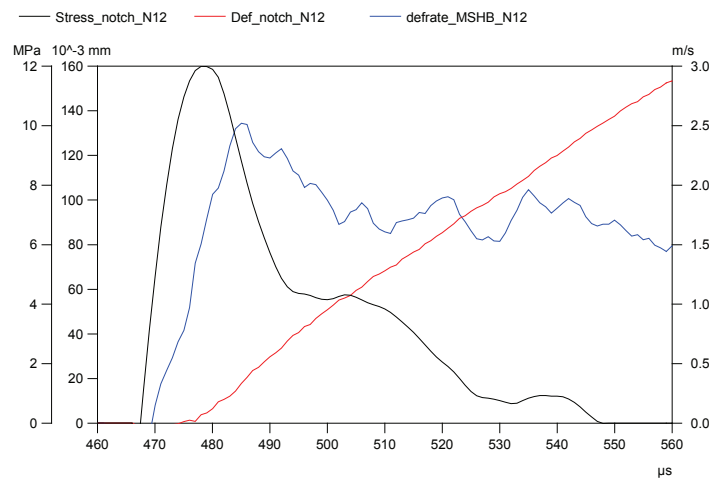


Figure 28 Records of MSHB test N12 for stresses ($\sigma(t)$ [MPa], axis left, black curve), deformation ($\delta(t)$ [10^{-3} mm], axis left, red curve), and deformation rate ($\dot{\delta}(t)$ [m/s], axis right, blue curve).

From the experimental results the structural inertia effects can be quantified that occur when the deformation rate increases during fracture. The deformation is recorded in real time and therefore the acceleration in the pre-peak non-linear phase can be determined. This is the phase in which inertia effects can contribute to the measured strength. For the example given in Figure 5 the pre-peak non-linearity in $\sigma(t)$ starts at approximately 473 μ s, when the deformation increases and micro-cracks start to form. The pre-peak ends at maximum of $\sigma(t)$ (approximately at 479 μ s, so $\Delta t = 6\mu$ s). The acceleration $\ddot{\delta}$ in this time frame is almost constant and for this particular test about $1.9 \cdot 10^5 \text{m/s}^2$.

To be able to determine the contribution of structural inertia in the fracture zone to the force equilibrium, we need information on the mass and therefore on the width of the fracture zone. Within a time frame Δt a width of $2 \cdot \Delta t \cdot C_p$ can be activated, C_p being the concrete sound velocity. Using $C_p=3500\text{m/s}$ the theoretical width will be within the range of 40mm. However, when considering the experimental results on the width of the fracture zone (L_{FZ} , Table 1), the final width is approximately 20mm. The width L_{FZ} of 20mm will be used to estimate the structural inertia contribution in the apparent dynamic strength of the MSHB tests. The deformation of the fracture zone will not be equally distributed, but concentrated around the final macro-crack (see Figure 4, left). Therefore, the mass of the fracture zone will not be fully activated. Combined with the recorded acceleration, only a mass fraction (b) should be taken into account. The contribution of the fracture zone inertia to the apparent strength is given by:

$$\Delta f_{i,dyn} = b \cdot L_{FZ} \cdot \rho \cdot \ddot{\delta}$$

The mass fraction b is unknown, so the contribution of inertia of the fracture zone to the observed strength for the MSHB and the SHB tests is given in Table 2 using different values for b.

Table 4 Contribution inertia fracture zone to apparent strength for the SHB and MSHB tests

Δft	b=0.1 [MPa]	b=0.2 [MPa]	b=0.3 [MPa]	b=0.4 [MPa]
Δft_{MSHB}	0.7	1.5	2.2	3.0
Δft_{SHB}	0.01	0.02	0.03	0.05

The analyses of the SHB and MSHB data show that the structural inertia of the fracture zone in the pre-peak response has a considerable effect on the strength increase for high loading rates, but up to a loading rate of 50GPa/s the inertia effects of the fracture zone can be disregarded.

Although the presented experimental results give a proper indication of the contribution of the inertia effects of the fracture zone, additional numerical research might be necessary to be able to accurately quantify the contribution of inertia to the apparent strength.

THE APPARENT FRACTURE ENERGY

The previous section addressed the effect of the structural inertia of the fracture zone on the apparent strength in the pre-peak phase. In this section the post peak response will be analysed in a similar way. The stress-deformation curve for post peak-response is schematized commonly into two branches, i.e. the steep branch directly beyond the peak and a moderate declining branch. The first branch is coupled to the phase of micro-cracking and the long tailed second branch represents the formation of the final macro-crack. The curves for all tested loading and curing conditions are given in Figure 6.

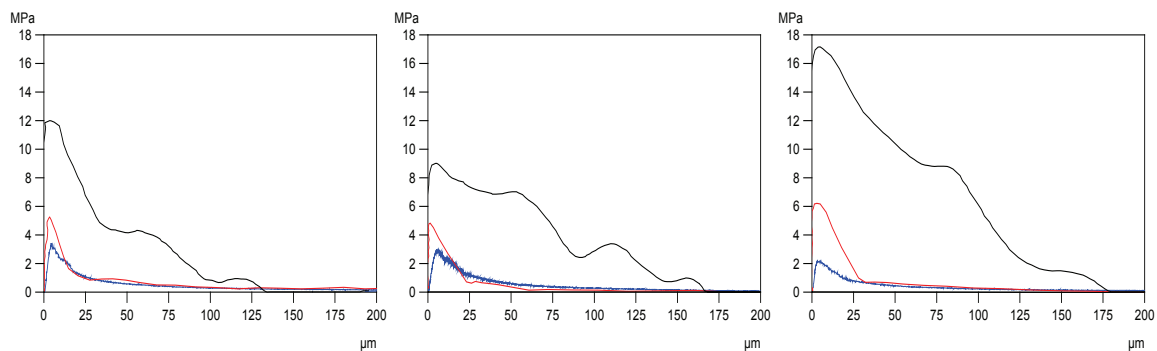


Figure 29 Stress-deformation curves for three curing conditions (normal-left; dry-middle and wet-right) for three loading rates (static-blue line; SHB-red line and MSHB black line)

The total length of the macro-crack is similar for all three loading rates (see Table 1), which indicates that the shape of second branch of the softening curve for different loading rates should be quite

similar. The experiments show, however, that the second branch of the softening curve is similar for static and SHB tests, but the tail of the MSHB tests is less steep (see Figure 6). The combination of no increase in macro crack length and still a difference in shape of the softening curve would imply that another mechanism contributes to the enhanced resistance, like for instance structural effects in the fracture zone. The inertia might delay the opening of the macro crack and will be recorded as additional resistance. In analogue with the pre-peak analysis, the deformation rate and acceleration is analysed. Four response stages are identified, see Figure 7. Note that the recorded “bumps” in the recorded softening branch are due to reflections in the “spall-part” of the specimen.

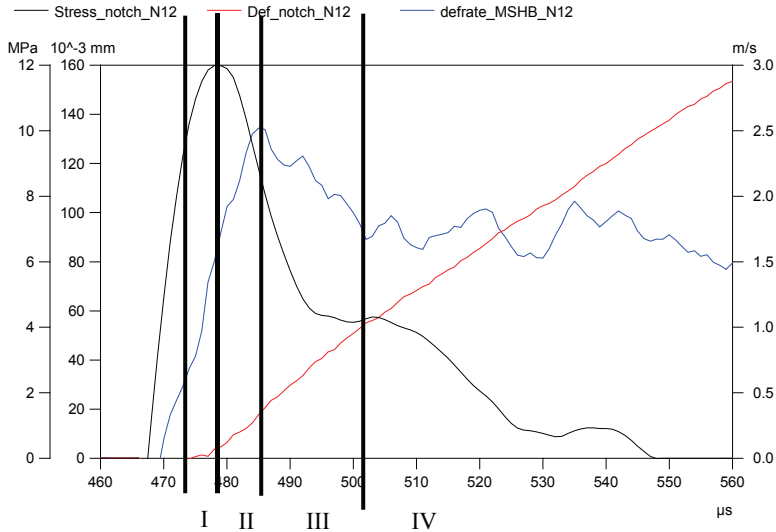


Figure 30 Post-peak analysis of the stress, deformation and deformation rate (MSHB test example). Records of MSHB test N12 for stresses ($\sigma(t)$ [MPa], axis left, black curve), deformation ($\delta(t)$ [10^{-3} mm], axis left, red curve), and deformation rate ($\dot{\delta}(t)$ [m/s], axis right, blue curve).

The deformation velocity increases, until the maximum apparent strength is reached (phase I). After reaching the maximum strength, the deformation rate increases furthermore over the first part of the softening curve (phase II). During the second part the deformation velocity drops (phase III) to a more or less constant value (phase IV). The inertia contribution to the post peak resistance is given in Table 3 for three mass fractions b .

Table 5 Contribution of inertia fracture zone to apparent tensile resistance in MSHB tests for different mass fractions b .

$\Delta ft_{inertia}$	Average Acc [$\cdot 10^5 \text{ m/s}^2$]	$b=0.2$ [MPa]	$b=0.3$ [MPa]	$b=0.4$ [MPa]
Pre-peak (phase I)	1.58	1.5	2.2	2.9
1 st post peak (phase II, acc)	1.11	1.0	1.6	2.1
2 nd post peak (phase III, dec)	-0.64	-0.6	-0.9	-1.2
3 rd post peak (phase IV)	+/-0.0	+/-0.0	+/-0.0	+/-0.0

The results show that the structural inertia of the fracture zone plays an important role in the pre-peak phase and the first branch of the softening curve. The inertia effects contribute to an increased strength and therefore a larger fracture energy. Due to the deceleration phase in the softening curve, the structural effects will decrease the apparent stresses and therefore the apparent fracture energy will even decrease in this phase. A remarkable observation. This means that the enhanced resistance found

in the tail of the stress-deformation curve must be due to another mechanism than structural inertia of the fracture zone.

The authors realize that the “acceleration recording” by differentiating $\delta(t)$ twice, is not accurate and filtering was necessary to limit the introduced noise. Nevertheless the trend in inertia contribution to the post-peak response can be determined. The correction procedure was applied for the whole stress-deformation curve of the MSHB tests. A representative result is given in Figure 8 together with the static and SHB curves. It is obvious when comparing the corrected stress-deformation curve at high loading rates with medium and static loading rates that concrete becomes more ductile in the high loading rate regime. After elimination of the inertia affects, the peak is still wider, the softening curve is less steep and the total fracture energy increases significantly at high loading rates.

From the crack pattern analysis (Table 1) it was observed that at high loading rates the number of micro cracks increased with a factor 1.3. To estimate their contribution to the fracture energy the “static” curve was scaled up proportionally using the factor of additional micro cracks (in 3D, the cracks increase with a factor 1.3^2 , equals to 1.7), see dark purple curve in Figure 8. The grey area in between the corrected stress-deformation curve, inertia of the fracture zone excluded, and the static curve with ‘70% more fracture energy due to micro cracks’ shows an increase in fracture energy due to additional resistance of the material, not being structural inertia of the fracture zone or additional micro-cracks. Most likely the additional post-peak resistance is due to the moisture in the pores. The analyses of the “dry” and “wet” test results will reveal more information on this statement (Vegt 2015).

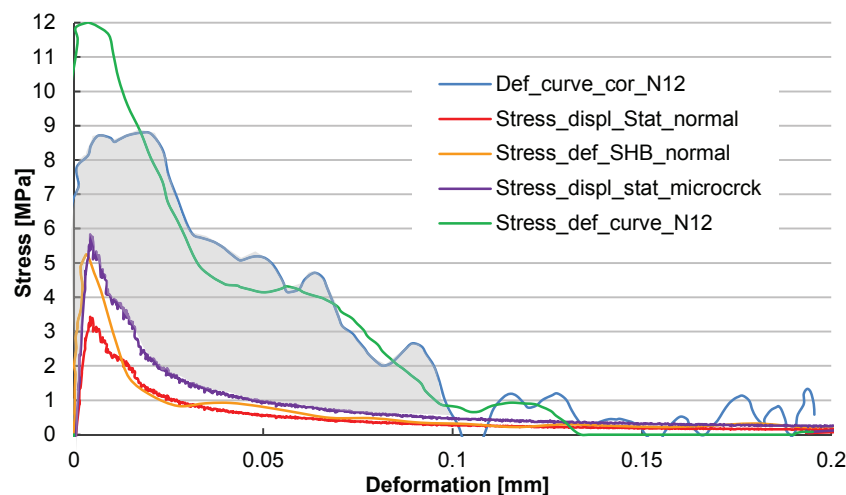


Figure 31 Corrected Stress-deformation curve for MSHB test N12 (light blue), compared with apparent stress-deformation curve (green), static stress-displacement curve (red), SHB stress-deformation curve (orange) and static stress-displacement with 70% more micro cracks (dark purple).

CONCLUDING REMARKS

The rate effects on concrete strength and fracture energy have been studied in an extensive experimental research programme. For static, intermediate and high loading rates the stress and deformation of the fracture zone are recorded real time. Afterwards, the fracture zone is studied and the length and distribution of the macro- and micro-crack are quantified by microscopic analysis. This data enables the reconstruction of the stress-deformation relation and the study of the mechanisms governing the concrete rate dependent behaviour.

In this paper the focus was on contribution of the inertia of the fracture zone to the apparent tensile strength and fracture energy. The presented data and analyses reveal that:

- Inertia of the fracture zone in the pre-peak response plays an important role in the high loading rate regime. This inertia seems to be responsible for a large part of the strength increase beyond loading rates of 50GPa/s.
- For loading rates up to 50GPa/s, the fracture energy, shape of the stress-deformation curve, width of the fracture zone and the amount of micro-cracking are hardly affected. The rate effect is restricted to the enhanced strength.
- At high loading rates (>50GPa/s), the length of the macro-crack does not change. The width of the fracture zone increases considerably, while the amount of micro-cracks increases only moderately. The fracture mechanics analysis showed that additional micro-cracking is possible, but only at higher loading rates (>45GPa/s).
- The pre- and post-peak response needs to be adjusted for structural inertia effects in the fracture zone. From the established data on deformation rate it can be concluded that this structural inertia effect is limited to the first part of the softening curve and can be ignored for the macro-cracking phase. If the structural inertia of the fracture zone is captured by the numerical simulation, its effect on strength and fracture energy have to be excluded from the constitutive model. In the constitutive model only the rate effects due to moisture contents and micro inertia should be included.

ACKNOWLEDGMENTS

The authors gratefully acknowledge the financial support of Foundation for Technical Science (STW) in the Netherlands.

REFERENCES

- Cadoni, E., Labibes, K., Albertini, C. and Berra, M. (2001). Strain rate effect on the tensile behaviour of concrete at different relative humidity levels. *Materials & Structures* 34: 21-26
- Cotsovos, D.M. and Pavlovic, M.N. (2007) Numerical investigation of concrete subjected to high rates of uniaxial tensile loading. *Int. J. Impact Eng*, doi:10.1016/j.ijimpeng.2007.03.006
- Erzar B., Forquin P. (2010). An experimental method to determine the tensile strength of concrete at high rates of strain. *Experimental Mechanics*, 50(7), pp. 941-955.
- Kipp, M.E. , Grady., D.E. and Chen, E.P. (1980) Strain rate dependent fracture initiation. *Int. Journal of Fracture*, Vol 16, pp 471-478.
- Malvar, J. and Ross, A.C. (1998). Review of strain rate effects in concrete. *ACI Materials Journal*. Technical paper no. 95-M73.
- Ožbolt, J., Sharma, A. and Reinhardt, H. W. (2011). Dynamic fracture of concrete – compact tension specimen, *International Journal of Solid and Structures*, 48, 1534-1543.
- Ožbolt, J. and Sharma, A. (2012), Numerical simulation of dynamic fracture of concrete through uniaxial tension and L-specimen, *Engineering Fracture Mechanics*, 85, 88-102.
- Ožbolt, J., Weerheijm, J, and Sharma, A. (2013), Dynamic tensile resistance of concrete-Split Hopkinson Bar Test, in VIII Int. Conf. on Fracture Mechanics of concrete and structures, FraMCoS-8, Toledo, Spain, March 2013.
- Reinhardt H.W., Rossi, P. and van Mier, J.G.M. (1990). Joint investigation of concrete at high rates of loading. *Mater Struct* 1190; 23:213-6
- Vegt, I., Weerheijm, J. and Van Breugel, K. 2007. The fracture energy of concrete under impact tensile loading- a new experimental technique. *CONSEC Conference June 2007, Tours, France*.
- Vegt, I., Weerheijm, J. and Van Breugel, K. 2006. Moisture content and the effect on dynamic concrete behaviour. *Proceedings of the 2nd Int. Conf. on Design and Analysis of Protective Structures, Singapore, 13-15 November 2006*.
- Vegt, I. (2015). Concrete in dynamic tension; the fracture process Doctoral thesis, Delft University of Technology (to be submitted)
- Weerheijm, J. et al. (2013) *Understanding the tensile properties of concrete*. Editor. Weerheijm.J. Woodhead Publishing 2013.